International Journal of Heat and Mass Transfer 107 (2017) 882–894

Contents lists available at ScienceDirect

International Journal of Heat and Mass Transfer

journal homepage: www.elsevier.com/locate/ijhmt

Heat loss prediction of a confined premixed jet flame using a conjugate heat transfer approach

S. Gövert [a,*], D. Mira [b,*], M. Zavala-Ake [b], J.B.W. Kok [a], M. Vázquez [b,c], G. Houzeaux [b]

[a] University of Twente, Faculty of Engineering Technology, Enschede, The Netherlands
[b] Barcelona Supercomputing Center (BSC-CNS), Barcelona, Spain
[c] IIIA-CSIC, Bellaterra, Spain

ARTICLE INFO

Article history:
Received 23 June 2016
Received in revised form 18 September 2016
Accepted 31 October 2016
Available online 5 November 2016

Keywords:
Conjugate heat transfer
Non-adiabatic turbulent combustion

ABSTRACT

The presented work addresses the investigation of the heat loss of a confined turbulent jet flame in a lab-scale combustor using a conjugate-heat transfer approach and large-eddy simulation. The analysis includes the assessment of the principal mechanisms of heat transfer in this combustion chamber: radiation, convection and conduction of heat over walls. A staggered approach is used to couple the reactive flow field to the heat conduction through the solid and both domains are solved using two implementations of the same code. Numerical results are compared against experimental data and an assessment of thermal boundary conditions to improve the prediction of the reactive flow field is given.

1. Introduction

Heat transfer is a key issue to evaluate the overall performance and life duration of practical combustion systems. The understanding of the temperature distribution in thermal devices is not only beneficial to improve particular operating conditions, but also to enhance aerodynamic, thermal design, and selection of appropriate materials for a given application. One of the main applications of aerothermal engineering is the design and development of propulsive systems such as Gas Turbines (GT) or Internal Combustion Engines (ICE). In such devices, the existence of heat losses influences the local gas temperature of the reacting layers affecting the kinetics of the reactions and also the formation of pollutants. In particular, in situations where abnormal combustion might take place, the effects of heat losses become even more important. In ICE, high and varying cylinder wall temperatures can induce undesired phenomena such as engine knock or rumble [1]. For GT's, the heat losses are not only important in the combustion chamber itself, but also on the high pressure turbine stages. The turbine inlet temperature is one of the key parameters to increase the thermodynamic efficiency [2,3], so improvements in the turbine blade cooling techniques and metallurgical advances contribute to the overall engine performance. However, with increasing turbine inlet temperatures, the accurate description of heat transfer in the combustor and the prediction of the temperature distribution at the combustor exit becomes even more important.

To achieve a good engine performance with low pollutant emissions and to ensure a full integrity and predictable lifetime of the system, an efficient management of heat loads must be undertaken. The local heat fluxes exchanged in the combustion chamber need to be evaluated and the wall local temperature must be known. This requires not only information of the mean temperature, but also its transient variations [4].

The present work addresses the prediction of the heat losses in a lab-scale combustor using a conjugate heat transfer approach. The test case that is used for the current investigation is a turbulent premixed jet flame that has been experimentally investigated by Lammel et al. [5] and has been subject of extensive numerical validation [6–9].

A sketch of the combustor is presented in Fig. 1 including a sectional view of the inlet section. The off-centre positioning of the jet exit induces the formation of a pronounced lateral recirculation zone which serves for flame stabilization. Due to the combustor design with major parts of the combustor walls exposed to the atmosphere, convective heat losses to the walls have a strong influence on the flow field and this is a distinctive feature of this burner. However, no measurements of the wall temperature are available and the exact heat transfer conditions are unknown. Because of these circumstances, the heat transfer through the walls has been modelled in all the previous investigations by the use of isothermal boundary conditions and under the assumption of uniform values along the entire combustion chamber. The applied values were

* Corresponding authors.
E-mail addresses: s.govert@utwente.nl (S. Gövert), daniel.mira@bsc.es (D. Mira).

http://dx.doi.org/10.1016/j.ijheatmasstransfer.2016.10.122
0017-9310/

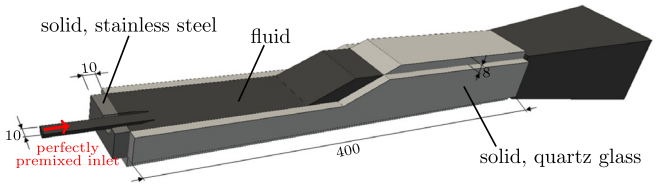

Fig. 1. Sketch of computational domain for fluid and solid including main dimensions in mm. A normal cut through the domain is used for the inlet section to enable a sectional view of the inlet pipe and to visualize the off-centre positioning of the jet exit. The location of the perfectly premixed inlet is indicated by the red arrow. (For interpretation of the references to colours in this figure legend, the reader is referred to the web version of this paper.)

based on visual estimation and the rough analysis of the ageing behaviour of the quartz glass walls. The applied temperature values for the wall boundary condition ranges from 800 K [8] over 1000 K [7,6] to 1273 K [9]. The large spreading of the applied boundary condition indicates the uncertainties in the modelling and the user influence on the heat loss prediction. Additionally, the assumption of uniform temperatures along the walls seems to be inappropriate. While relatively high wall temperatures are expected downstream of the jet exit where the flame approximates the walls, significantly lower temperatures can be expected in the lateral recirculation region where long residence times of the combustion products lead to strong convective heat loss [5].

The objective of this paper is to overcome the heat transfer modelling limitations of the aforementioned simulations and to fully characterize the heat transfer in the combustor. Therefore, the influence of radiative heat exchange with the walls and the heat conduction through the combustor walls are included in the numerical model presented in the current work. In order to accurately predict the internal wall temperatures in the combustor and to reduce the user influence, a Conjugate Heat Transfer (CHT) approach is applied. In general, CHT problems can be solved either using monolithic solvers, in which the different physical processes are solved simultaneously in one solver, or in a staggered approach in which different solvers are coupled at an interface to form a new aggregated solver. The latter approach is used throughout this work. The resolution of conjugate heat transfer problems is challenging for computational methods due to its inherent coupling between the scales governing the fluid motion and the heat conduction through solid materials. The spatial and temporal scales of heat transport in the fluid and the solid differ by orders of magnitude, which complicates the numerical simulation. Therefore, a Dual Heat Transfer (DHT) approach is applied to compute steady temperature distributions in the solid and a strongly coupled CHT approach is used to investigate the transient characteristics of the coupled problem.

The coupled fluid–solid problem is analysed in several steps. Initially, the mean temperature distribution at the fluid boundary is determined based on the dual heat transfer approach in combination with RANS turbulence modelling. As several coupling iterations are required in the DHT approach, the application of RANS allows the prediction of a non-uniform wall temperature distribution and an initial guess for the LES at significantly reduced computational costs. Even though it is difficult to exactly match the mean temperature distribution between RANS and LES, the proposed approach offers a practical way to compute an initial guess for the final LES. Different boundary conditions for the temperature at the outside walls are tested and their influence on the temperature distribution inside of the combustion chamber is explored. In a next step, the non-uniform temperature field that is determined by the DHT approach is applied to a transient LES simulation as thermal boundary condition. The results are compared to the baseline configuration in which constant and uniform thermal boundary conditions are used. Thereby, the influence of the local variation of the wall temperature on the flow field and the flame structure can be determined. Afterwards, transient effects of the heat transfer coupling, like thermal penetration and the low-pass filtering of the heat flux by the solid, are evaluated based on a strongly coupled CHT simulation. To overcome the problem of the multi-time-scale problem discussed above, the simulation is initialized using the developed fields from the DHT simulation. Finally, the influence of radiative heat exchange with the walls is analysed including the application of a radiation model. The flame radiation is accounted for using the assumption of optically thin transfer between the hot combustion gases and the cold surroundings [10].

The remainder of the paper is organized as follows. First, the modelling approach is presented in Section 2 including the fluid modelling (Section 2.1), the thermal modelling of the structure (Section 2.3) and a detailed discussion of the different CHT coupling algorithms (Section 2.4). Afterwards, the experimental setup is presented in Section 3. The numerical setup of the test case is discussed in Section 4. Then, the simulation results are presented and discussed in Section 5 before the final conclusions are given in Section 6.

2. Modelling approach of the coupled fluid and solid domain

In this section, the modelling approach is presented. First, the modelling of the fluid flow is briefly introduced. Subsequently, the thermal modelling of the solid is presented, followed by the different strategies for the coupling of fluid and solid.

2.1. Fluid modelling

The simulation of the fluid flow is characterized by the modelling of non-adiabatic turbulent combustion. In the following section, the applied fluid modelling strategy is summarized. For an extensive description of the combustion modelling and numerical treatment, the reader is directed to [6].

A flamelet based chemistry tabulation is employed in which the thermochemical properties originate from a laminar one-dimensional flame structure. This chemistry reduction method is known as Flamelet Generated Manifold (FGM) [11] or Flame Elongation of ILDM (FPI) [12]. In the current work, the reaction source term S_c as well as the transport coefficients of the reacting mixture are tabulated based on the solution of one-dimensional premixed flame simulations, which are carried out using CHEMKIN PREMIX [13,14]. The GRI-Mech 3.0 reaction mechanism [15] with detailed transport and thermodynamic properties is used. To account for the effect of heat loss on the chemical reaction rates, several flamelets at different enthalpy levels are tabulated to accurately describe the combustion process [16]. The different flamelets are computed by the use of burner stabilized one-dimensional flames with conductive heat losses to the burner inlet [17]. The flamelets are parametrized in terms of a Reaction Progress Variable (RPV) and the normalized enthalpy scalar i. Further details about the choice of the reaction progress variable and the enthalpy normalization can be found in [6].

Turbulence-chemistry interaction is accounted for by integration over a presumed-shape Probability Density Function (PDF). Commonly, the statistical correlations between the RPV and the enthalpy scalar are assumed to be negligible due to the normalization procedure and the averaging process is done using a factorized joint PDF approach. A β-PDF shape is used to define the turbulent effects of the RPV, since it is assumed that moderate levels of fluctuations occur for this case [18]. Due to the almost linear dependency of the species mass fractions and temperature on the

enthalpy scalar i, turbulent fluctuations in i are assumed to have only a small effect [19] and are neglected. This has the advantage that only the mean of the enthalpy scalar is required and higher moments do not need to be computed.

A low-Mach number approximation of the conservation equations of mass, momentum and enthalpy is solved along with transport equations for the mean and variance of the reaction progress variable to describe the state of chemical reaction. The normalized enthalpy scalar is coupled directly to the non-normalized enthalpy and no additional transport equation is required. The temperature is determined by the conservation of enthalpy and is computed by solving a polynomial expression for the enthalpy. The polynomial coefficients depend on the local composition only and mixture-averaged coefficients are tabulated in the database as a function of the controlling variables.

While the unity Lewis number assumption is used for the determination of the laminar diffusion coefficient, the unclosed term of the filtering operation is modelled using the eddy diffusivity hypothesis [20] with a turbulent Schmidt number of $Sc_t = 0.9$. The subgird-scale turbulence contribution in the LES is determined based on the Wall-Adapting Local Eddy-viscosity model (WALE) [21] while the k-ω-Shear Stress Transport (SST) [22] turbulence model is used to determine the unclosed turbulence terms for the RANS simulations.

2.2. Radiation modelling

In Section 5.4, the impact of radiative heat transfer is investigated based on the application of a radiation model using the optically thin flame assumption. In that case, a volume source term is added to the enthalpy transport equation describing the divergence of the radiative heat flux. This approach can be seen as the net outflow of radiant energy per unit volume determined by the balance of absorbed and emitted radiant energy. The assumption of optically thin transfer between the combustion gases and the surroundings is used to determine the radiation source term [23,24] as follows:

$$\nabla \cdot \dot{q}_R = 4\sigma a_p(T,p)T^4 - 4\sigma a_{mp}(T_w,T,p)T_w^4 \tag{1}$$

where σ is the Stefan–Boltzmann constant, T_w is the temperature of the surrounding walls and T is the local fluid temperature. a_p and a_{mp} are the mean Planck absorption coefficient and the modified mean Planck absorption coefficient, respectively. The first term on the right hand side accounts for the radiative energy emitted by the gas, while the second right hand side term accounts for the absorption of radiative energy emitted by the surrounding walls. The mean Planck absorption coefficient is determined by a summation over all the species K as:

$$a_p(T,p) = \sum_{k=1}^{K} p_k a_{p,k} \tag{2}$$

where p_k and $a_{p,k}$ are the partial pressure and the absorption coefficient of species k, respectively. $a_{p,k}$ is only function of the temperature and computed based on a polynomial fit. The polynomial coefficients used in the current work are taken from Chen et al. [25]. CO_2 and H_2O are assumed to be the main radiating species and the influence of other species is neglected.

In general, calculation of radiation energy absorbed by the gas involves an integration over wavelength, view angle and path length and depends therefore on the local conditions of the entire combustion chamber. Using the assumption of optically thin flames, a modified mean Planck absorption coefficient can be defined and used for the computation of the absorbed energy. An approximated relation between the modified mean Planck absorption coefficient and the mean Planck coefficient [23] is given by the following relation:

$$a_{mp}(T_w,T,p) = \frac{T_w}{T} a_p(T_w,p) \tag{3}$$

2.3. Thermal modelling of the structure

The solid domain is treated as a rigid body for which the heat equation is solved. In absence of volumetric sources, the energy equation in the structure is defined as:

$$\rho c_p \frac{\partial T}{\partial t} = \nabla \cdot (\lambda \nabla T) \tag{4}$$

Constant values are used for the density of Quartz glass and stainless steel (2200 kg m^{-3} and 1750 kg m^{-3}, respectively). However, the temperature dependency of heat capacity and heat conductivity are taken into account by the use of polynomial functions. The polynomial coefficients for the Quartz glass are based on the experimental measurements of Kelley [26] for the specific heat capacity and Sergeev et al. [27] for the heat conductivity. The properties of stainless steel are based on the EN 1993 [28]. Even though the relation for the heat conductivity of quartz glass is designed for temperatures up to 800 K, it will be used for higher temperatures as well at the cost of slightly increased deviation for the high temperature range.

2.4. Conjugate-heat transfer approach

The coupling of fluid and solid domain is achieved by the exchange of information at shared boundaries. To guarantee a full two-way coupling, the heat flux over the boundary is extracted in the fluid domain and supplied as a boundary condition in the solid domain. In a second step, the surface temperature is transferred from the solid to the fluid domain. To achieve a high accuracy and lower influence of mesh resolution, the computation of the heat flux is based on exchanging the global heat flux from the enthalpy equation, which is defined as the integral of the heat flux over the wall area interpolated locally at the nodes of the boundary [29].

One of the challenges of the application of conjugate heat transfer modelling in the framework of turbulent combustion is the vast difference in time scales associated to heat transport in fluid and solid [30]. A conductive time scale for the solid can be defined as:

$$\tau_s = \frac{L}{\mathrm{Le}} = \frac{L^2}{D_s} = \frac{L^2}{\lambda/(\rho c_p)} \tag{5}$$

in which L is a characteristic solid length (the wall thickness for the current case), $\mathrm{Le} = \frac{\lambda}{\rho c_p L}$ is the Lewis number for the solid and D_s is the solid heat diffusivity. λ, ρ and c_p are the heat conductivity, density and specific heat capacity of the solid, respectively. In the fluid, the combustion time scale at which heat is produced is estimated on basis of the flame thickness δ_l and the flame speed s_l as:

$$\tau_c = \frac{\delta_l}{s_l} \tag{6}$$

The characteristic time scales of the solid are usually some orders of magnitude larger than the combustion time scales. For the current case, the conduction time scale of the solid is about $\tau_s \approx 84$ s, while the combustion time scales take values of the order of 10^{-4} s . Under such conditions, the solid acts like a low-pass filter on the heat flux fluctuations. Due to the different time scales, a synchronization of the physical time between solid and fluid domain is out of scope for the determination of fully developed solution fields [1]. The physical time necessary for a developed

solid solution is out of reach for the fluid due to the small time scales characterising the flow and the long physical time to influence mean temperatures in the solid domain.

To overcome such situations, different coupling approaches are applied and combined in the course of the paper. A dual heat transfer method is used to obtain fully developed solutions of the mean temperature distribution at the fluid boundary. This will be used to obtain RANS solutions of the flow field using different boundary conditions in the outer wall. As the overall mean temperature will not significantly change in time, these temperature distributions will be used as a starting solution to study transient thermal effects in LES using a strongly coupled conjugate heat transfer simulation.

In the dual heat transfer approach, the solvers of the individual domains are fully converged independently to reach a steady state. Time-averaging is applied in case of transient phenomena. Only the fully converged solution at the interface is used as a boundary condition in the other domain. The application of this approach is well suited to obtain a steady state solution of the coupled problem in cases where the characteristic time scales differ significantly between solid and fluid [1]. If the conduction time scale of the solid is significantly higher than the characteristic combustion time scale, the solid filters out the high frequency fluctuations and these small scales are damped. In the dual heat transfer approach, the fluid and solid are computed sequentially. The fluid domain is computed with an initially uniform temperature distribution and the locally resolved wall heat flux is obtained. The temperature field in the solid is computed under consideration of the heat flux from the fluid domain. The new wall temperature distribution from the solid domain is used as a boundary condition in the fluid domain and the loop is continued until the exchanged fields are converged. Using a dual heat transfer approach, significant savings in terms of the computational requirements can be obtained.

However, transient phenomena are filtered out and a strongly coupled conjugate heat transfer approach needs to be applied in cases where time dependent aspects of the heat transfer are important. In this case, fluid and solid simulation are synchronized in physical time and the interface heat flux and temperature is exchanged at every time step.

3. Experimental setup of the test case

The test case that is used to investigate the influence of heat transfer modelling on the reactive flow solution corresponds to an experimental facility at the German Aerospace Center (DLR). The investigated operating point is part of a test series of measurements conducted by Lammel et al. [5]. The test case consists of a premixed turbulent jet flame that is confined in a rectangular combustion chamber. The combustor is operated at atmospheric pressure. A lean mixture of methane and air at equivalence ratio 0.71 is injected into the combustor through a circular pipe with diameter $d = 10$ mm. A pronounced lateral recirculation zone is obtained by the off-centre positioning of the jet nozzle and the recirculation of the hot combustion products establishes the flame stabilization. The premixed fuel–air mixture is injected with an inlet velocity of 90 m/s and a temperature of 573 K.

The walls of the combustion chamber are made of synthetic quartz glass with a thickness of 8 mm. The quartz glass allows for the optical access, that is required for laser-based measurements. The walls are bevelled at the corners and equipped with a sealing, such that the flame only is in contact with the quartz glass. The walls are mounted at the corners by the use of a support frame. In the streamwise direction, the combustion chamber walls consist of two 200 mm segments with narrow (2×5 mm) flanges of stainless steel. The burner base plate is 10 mm thick and made of stainless steel. It is mounted on the water cooled nozzle holder.

Even though no measurements of the wall temperature are available for the current test series, some conclusions can be drawn from a similar test case with different geometrical details and thinner walls. The temperature at the inner walls exhibits significant spatial variations. While a temperature of about 873 K could be expected upstream of the flame location, a strong temperature increase in the area of the flame impact up to 1273 K is possible. Based on the observed degradation level of the quartz glass, higher temperatures are unlikely. Outside of the combustor, the surrounding air is convected away by the use of a ventilation system and the streamwise temperature gradient over the combustor walls is quite large. For the test case with different geometrical dimensions and thinner walls, the outside wall temperature was measured and values at the level of 873 K were obtained. Along the walls, a flat profile was obtained with only little spatial variation [31].

4. Numerical setup

In the current work, the parallel multi-physics code Alya [32] is used to compute the solution fields for both, structure and fluid. Also the coupling between the domains and the exchange of the interface quantities is conducted by internal algorithms of the code. Alya is based on the Finite Element method using the Variational Multiscale Stabilization (VMS) approach [33] and is designed for large-scale parallel applications [34]. The spatial discretization of the modelling equations is based on linear finite elements and a second-order backward Euler time integration scheme (BDF2) is used.

The computational domain for the fluid includes the combustion chamber, the inlet nozzle and part of the inlet pipe. The combustion chamber extends up to 40 nozzle diameters, while a total of 7 nozzle diameters of the inlet pipe is included to reduce the influence of the inlet boundary condition on the turbulent flow field. For the modelling of the heat conduction in the solid, the domain includes the base plate and the quartz glass windows. The burner was specifically designed such that the hot gases are almost entirely in contact with the quartz glass walls. Due to the very small surface area of the frame, that is exposed to the fluid, only little influence on the temperatures inside of the combustor are expected. Therefore, the frame holder in the corners and the flanges of the segment connections are neglected in the structural model and the normal gradient at the side faces of the windows is set to zero. In Section 1, an overview of the fluid and solid domain including the main geometrical dimensions is presented in Fig. 1.

The same meshes are used for all the results presented in this paper. In total, the unstructured mesh for the fluid simulation consists of about 9.13 M elements and is presented in Fig. 2. The cell size in the inlet pipe and the flame region is about 0.08d and gradually coarsens in the downstream regions towards the outlet. A total number of 10 prism layers are added at all wall boundaries in order to capture the strong gradients in the boundary layer. The size of the first element at the wall is chosen such that the y^+ value in the combustion chamber, where the heat transfer to the walls is considered, remains below unity. The size of the prism elements increases in the wall normal direction following a log law with a growth rate of 1.1. Due to the small elements normal to the walls, no wall functions are required.

No-slip boundary conditions are set for the velocity at the walls. The inlet boundary conditions are set with top-hat profiles for enthalpy and progress variable, while a special treatment is required for the inlet velocity profile in the LES simulations. In order to obtain a turbulent flow field at the inlet plane of the flow domain, a precursor LES simulation of an infinite pipe flow is performed in a pre-processing step and the velocity components are sampled at the inlet plane of the combustor simulation at every

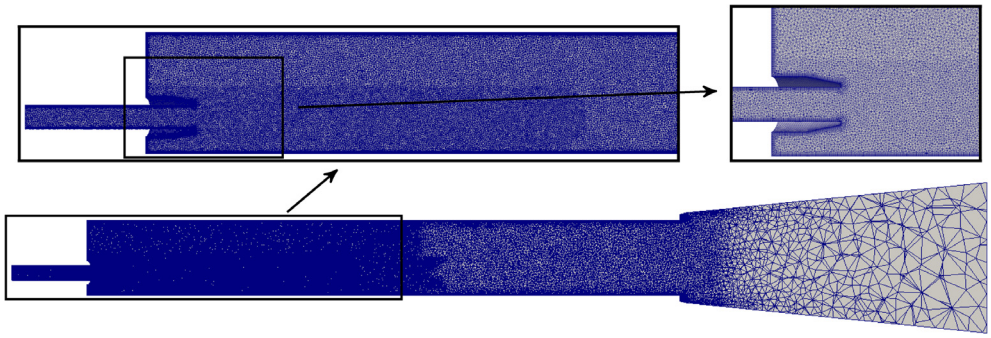

Fig. 2. Computational mesh for the fluid including close up views of the mesh refinement in the flame region and the jet exit.

time step. The result is a database of the spatially resolved time-series of the inlet velocity that is read during runtime in the reacting LES simulation. The domain has been extended in the streamwise direction coarsening the grid to allow for the formation of a buffer zone before reaching the outlet where outflow conditions are applied for all variables.

The mesh for the structure consists of 13.44 M prism elements and is shown in Fig. 3. The nodes at the fluid–solid interface are matching in order to avoid interpolation errors. A total of 40 elements are distributed in the direction normal to the heat flux following a log law with a growth rate of 1.15. While very small elements are needed close to the fluid–solid interface to account for the small thermal penetration depth and the steep temperature gradients [35], larger elements are located close to the outside walls. The element sizes in the normal direction range from 4.5 µm at the fluid boundary to about 1 mm at the outside boundary.

Isothermal boundary conditions are used at the outside walls of the solid and the influence of the respective value is analysed in Section 5.1. At the coupling interface, the heat flux from the fluid is imposed and the wall temperature is transferred back from the solid to the fluid.

The time step in the LES is set to 5×10^{-6} s which results in a CFL number of about 6 in the flame region. To remove the influence of initialization effects, the averaging process is started after 6 flow through times based on the inlet velocity. The flow was then time-averaged for a total of 24 flow through times based on the inlet velocity.

5. Results

In this section the results of the numerical simulations of this test case are presented and discussed. The analysis includes the assessment of the principal mechanisms of heat transfer in this combustion chamber: radiation, convection and conduction of heat over walls. The major characteristics of the studied test case can be extracted from the time averaged fields presented in Fig. 4. The time averaged fields of axial velocity, reaction progress variable and temperature are presented for the baseline LES in which a constant isothermal wall boundary condition is applied. Furthermore, the origin of the used coordinate system and the location for data sampling for the quantitative comparison are added in the figure. The test case is characterized by a strong lateral recirculation zone due to the off-centre positioning of the jet exit as indicated by the axial velocity. The field of the reaction progress variable reveals that the chemical reactions occur in the jet shear layers. Hot combustion products are transported back upstream and serve for flame stabilization. Due to the long residence times in the recirculation zone, the convective heat losses are high in this region and relatively low temperatures are observed.

The remainder of the results section is organized as follows. The first subsection is focused on the coupled fluid–solid heat transfer

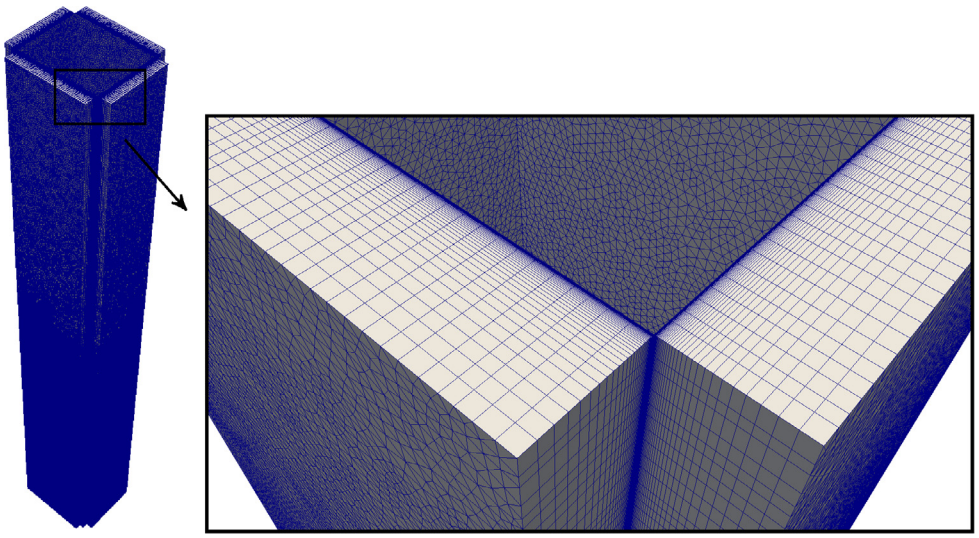

Fig. 3. Computational mesh for the solid including close up view of the mesh inflation at the fluid–solid interface.

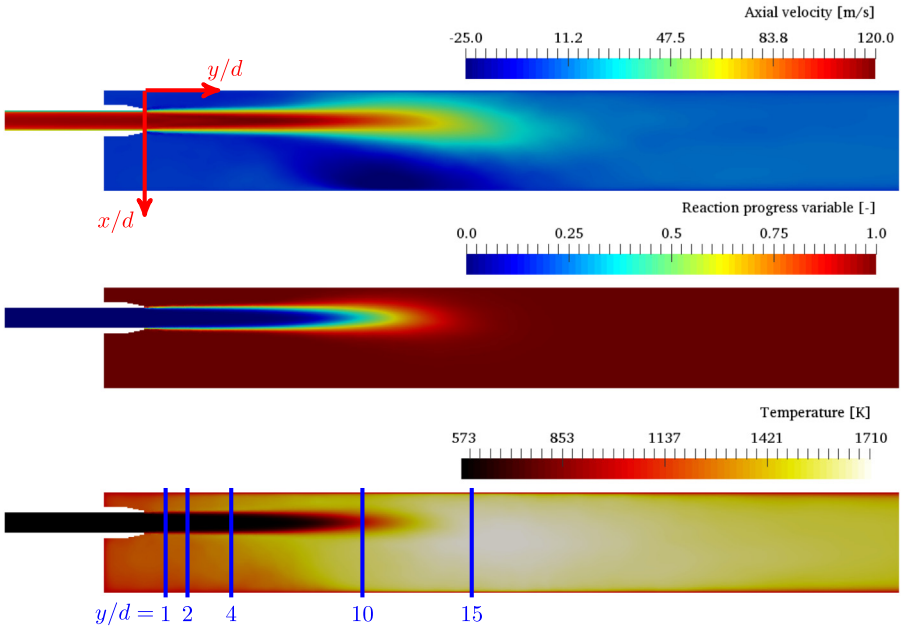

Fig. 4. Time averaged fields of axial velocity (top), reaction progress variable (middle) and temperature (bottom) for the baseline LES. The origin of the coordinate system is indicated in the top figure while the locations of data sampling for the quantitative comparison are indicated by the blue lines in the bottom figure. (For interpretation of the references to colour in this figure caption, the reader is referred to the web version of this article.)

problem and the analysis of the influence of the outside wall temperature on the results of the coupled problem. The coupling methodology for this case is based on a dual heat transfer approach in the context of RANS. The second subsection is focused on the description of the influence of the non-uniform temperature distribution at the fluid–solid interface in the context of LES. Afterwards, the results for a strongly coupled unsteady CHT simulation are presented with emphasis on the analysis of the transient effects of the thermal fluid–structure interaction. Finally, the influence of the radiative heat exchange with the environment and the influence of radiation in the prediction of the gas temperature within the combustion chamber is investigated. All previous investigations of this confined jet flame [8,9,7,6] have neglected these effects, but this will be examined here. For simplification, the structure is not included in the numerical model for this final step, but LES results including the radiation model are compared to the baseline case, in which radiative heat transfer is neglected.

5.1. Influence of the thermal conditions of the structure

The assumption of a constant uniform wall temperature in the fluid domain has been used throughout previous modelling attempts of this confined jet flame. In the present work, the heat conduction in the solid is included to relax this assumption. Nevertheless, a thermal condition needs to be applied to the outside wall of the combustor. As discussed in Section 3, the boundary condition for the outer wall of the solid is most accurately approximated by the use of an isothermal and uniform temperature condition. However, the actual value has not been measured and still remains unknown. Therefore, the impact of the outside wall thermal condition on the temperature distribution inside the combustion chamber is analysed by a variation of the applied boundary value. Due to the time-scale deviation of fluid and solid that was discussed in detail in the introduction, a dual heat transfer approach is applied in combination with RANS simulations to obtain mean interface fields in an efficient manner.

As described in Section 2.4, the DHT approach is based on the separate solution of fluid and solid domains. The coupling is achieved by the exchange of interface variables. In this approach, the convergence of the coupled simulation does not only depend on the convergence of the individual solvers, but also on the exchanged variables at the fluid–solid interface. Different criteria for the interface convergence are presented in Fig. 5 for a reference case with an outside wall boundary condition of $T_{out} = 900$ K. The convergence behaviour of the other conditions is comparable, so it is not shown here. The first criterion was based on the L_2-norm of the residual of the interface variables:

$$L_2^{res} = \frac{\|\phi^n - \phi^{n-1}\|}{\|\phi^n\|} \tag{7}$$

where ϕ represents either temperature or heat flux fields at the coupling interface and $\|.\|$ is the L_2-norm. This is shown in Fig. 5a. Within 5 coupling iterations, the drop in the residual for both fields is about an order of magnitude and the interface solution is assumed to be converged. An additional measure of the convergence of the interface quantities is the development of the mean temperature and mean heat flux values as illustrated in Fig. 5b. While the changes in the mean values are significant in the first coupling iterations, they hardly change after 4–5 iterations. Based on the aforementioned criteria, the coupled simulation converges within about 5 coupling iterations.

The influence of the boundary condition at the outside wall on the temperature distribution in the combustor can be obtained by comparison of the temperature profiles for different boundary values at the outside wall. The comparison for the temperature range from 800 to 1000 K of the outside wall boundary is presented in Fig. 6. The profiles for the fluid domain are extended by addition of the temperature development across the chamber walls. The conduction through the walls leads to an almost parallel temperature development in the walls for the different boundary conditions. Although, the temperature development is not exactly linear. This has the effect that the 100 K temperature difference at the outer walls between the different cases is reduced at the inner walls seen by the fluid.

In the fluid part, the cold region is hardly affected by the variation of the outside wall boundary condition and also the flame

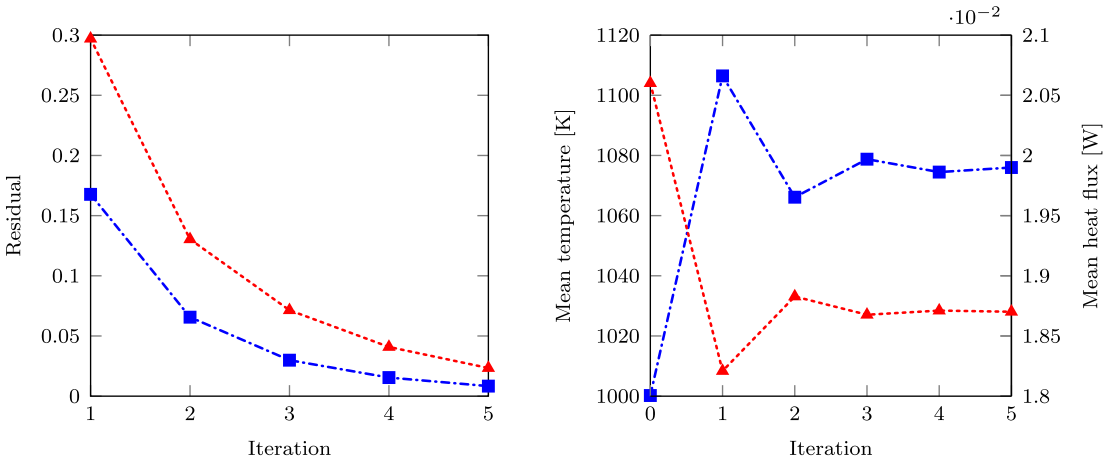

(a) Residual based on L2-norm (b) Mean values

Fig. 5. Convergence criteria of the temperature (-■-) and heat flux (-▲-) fields at the fluid–solid interface for $T_{out} = 900$ K.

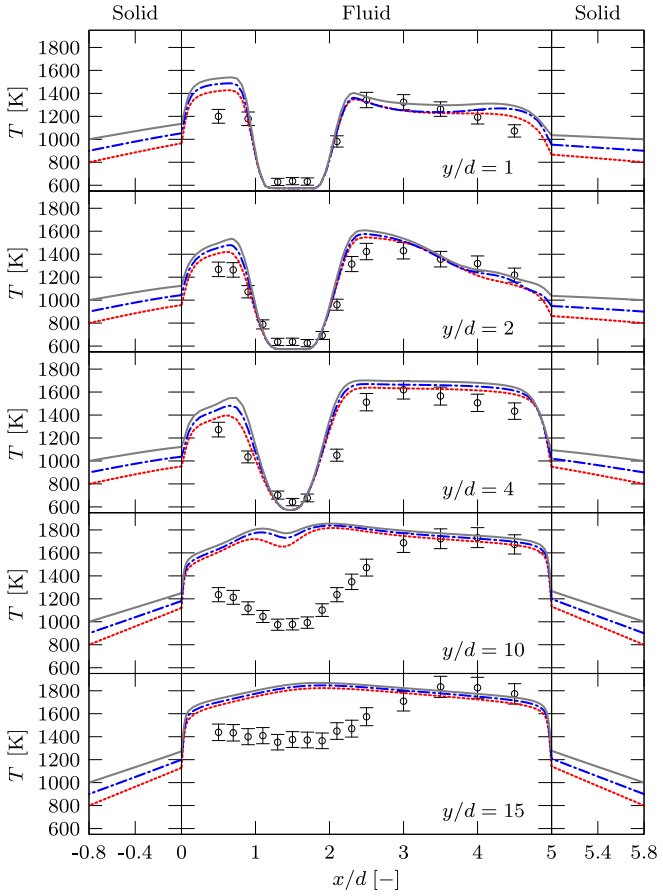

Fig. 6. Influence of the outside wall boundary condition on the temperature distribution in fluid and solid. Experiments (○), $T_{out} = 800$ K (·····), $T_{out} = 900$ K (-·-·-) and $T_{out} = 1000$ K (——).

front does not show any sensitivity to the wall condition. However, in the hot regions and the recirculation zone the influence is the highest and the temperature reduces nearly linearly with the wall boundary values. As example, the temperature at the fluid–solid interface is presented for the case of $T_{out} = 900$ K in Fig. 7. Independently of the actual value applied at the outside wall, the deviation of the temperature at the inner wall seen by the fluid is significant with a maximum deviation of about 350 K between hot and cold regions. Therefore, the assumption of uniform wall temperature can be considered inappropriate.

5.2. Non-uniform wall temperature

It is shown in the previous section, that by including the heat conduction through the walls in the numerical model, a significant spatial variation of the temperature at the fluid–solid interface is observed. Based on the DHT approach in the context of RANS, a non-uniform wall temperature distribution was determined. The boundary values were extracted from the results of the DHT simulation with an outside wall boundary condition of $T_{out} = 900$ K and applied as thermal boundary condition to an unsteady LES. A comparison of this LES simulation to the baseline case, in which a uniform wall temperature of $T_w = 1000$ K is used as isothermal boundary condition is presented here. Profiles of the mean temperature and the Root Mean Square (RMS) values of the LES with the non-uniform wall boundary condition are compared with the baseline case in Fig. 8.

The non-uniform boundary condition improves the mean temperature prediction in major parts of the domain. In general, the temperature level in the combustor is increased, though the overall deviation from the mean temperature predictions does not exceed 150 K in any region of the combustor. The largest influence is observed in the hot regions along the downstream profiles where the temperature is increased about 100 K in comparison to the baseline case. Interestingly, the temperature in the recirculation zone in the upstream profiles is almost identical close to the wall but the deviation increases further away from the walls towards the reacting layers where the predicted temperature is higher for the non-uniform boundary case. The flame location and length reveals no sensitivity to the thermal boundary condition and remains nearly unchanged. While the non-uniform boundary condition improves the prediction in most of regions, in the small recirculation zone where the flame is close to the walls, the temperature is overpredicted and the agreement with the experimental reference is reduced.

In general, the fluctuations of the temperature are increased by the use of the non-uniform wall condition. Especially in the recirculation zone the RMS level is significantly increased, though it is still underpredicted. While the mean temperature profiles reveal a similar behaviour close to the walls, the temperature fluctuations are affected by the wall boundary condition in the entire

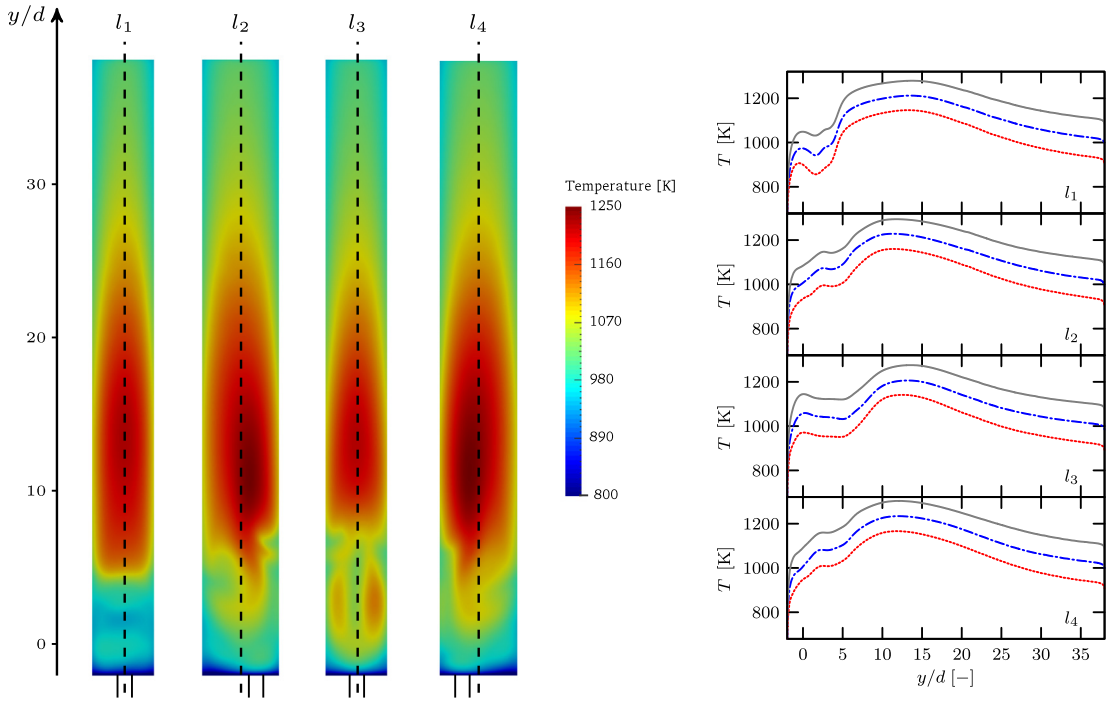

Fig. 7. Left: Non-uniform temperature distribution at the fluid–solid interface for $T_{out} = 900$ K. The location of the inlet pipe is indicated. l_1 corresponds to the wall close to the recirculation zone, further away from the jet exit while l_3 is the short wall close to the jet exit. Right: Profiles of wall temperatures along l_1 - l_4 for the different outside wall boundary conditions. $T_{out} = 800$ K (·····), $T_{out} = 900$ K (-·-·-) and $T_{out} = 1000$ K (——).

combustion chamber. The temperature fluctuations are not only affected close to the walls, but in all hot regions.

5.3. Transient behaviour

In the previous section, the influence of the non-uniform temperature distribution at the inside walls of the combustion chamber on the distribution of the gas temperature has been investigated. However, the wall boundary condition in the LES simulation was still defined as a fixed Dirichlet condition. In this section, the LES simulation of the fluid flow in the combustion chamber will be combined with a solver for the heat conduction through the walls in a strongly coupled CHT approach. Thereby, the temperature condition at the fluid–solid interface is relaxed and determined by the coupled fluid–solid problem. As discussed in Section 2.4, it is not feasible to obtain converged fields for the fully coupled problem due to the very different time scales in the fluid and solid domain. To account for this problem, it is important to define a suitable initialization of the fully coupled CHT simulation. To this extend, it is assumed that the steady fields obtained by the DHT approach, which is discussed in the previous sections, do not differ significantly from the mean solution fields in the fully coupled CHT simulation. Based on this assumption, the DHT solution is used to define the initial temperature distribution in the solid and the solution fields of the LES simulation with non-uniform wall temperature are used to initialize the fluid solver. Temperature values at the wall are expected to fluctuate along the given mean values, so no major changes in mean temperature at the interface are expected here.

In Fig. 9, the mean and RMS temperature of the fully coupled CHT simulation is compared to the baseline case and the LES simulation with non-uniform Dirichlet boundary condition. The mean temperature distribution of the strongly coupled CHT simulation reveals only very small differences in comparison to the LES simulation with non-uniform temperature boundary condition. However, significantly higher RMS values are predicted in the recirculation region by the CHT simulation. In this region, a maximum difference of about 80 K is observed by application of the relaxed thermal boundary condition. The prediction of the temperature fluctuations is significantly improved and closer to the experimental reference, even though the RMS values are still slightly underpredicted. No significant differences are observed for the downstream profiles and the region where the flame is located close to the wall. The improved prediction of the temperature fluctuations is caused by the relaxed temperature boundary condition at the wall. However, similar to the cases with fixed wall temperature, the RMS value directly at the wall tends towards zero for the CHT case as well.

Due to the large conductive time scale, only small fluctuations occur in the solid. The maximum values are located at the fluid–solid interface but do hardly exceed values of 2 K. This is in agreement with the low RMS value at the fluid–solid interface observed for the fluid domain (see Fig. 9). The small temperature fluctuations at the solid wall can be explained by the thermal activity ratio. The thermal activity ratio is a parameter that can be used to explain the thermodynamical behaviour of a fluid–solid interface and is defined as:

$$K = \sqrt{\frac{(\rho c_p \lambda)_{fluid}}{(\rho c_p \lambda)_{solid}}} \tag{8}$$

When K tends towards infinity, the wall temperature fluctuations reveal an iso-flux boundary behaviour (corresponding to maximum fluctuations), while for K approaching zero, the interface behaves like an isothermal wall with no fluctuations of the temperature [29,36]. The thermal activity ratio for the current case is about 2×10^{-3}. This very small value indicates that almost all the temperature fluctuations will be damped.

The frequency dependent damping behaviour of the solid can be analysed by evaluating the time series obtained at monitoring

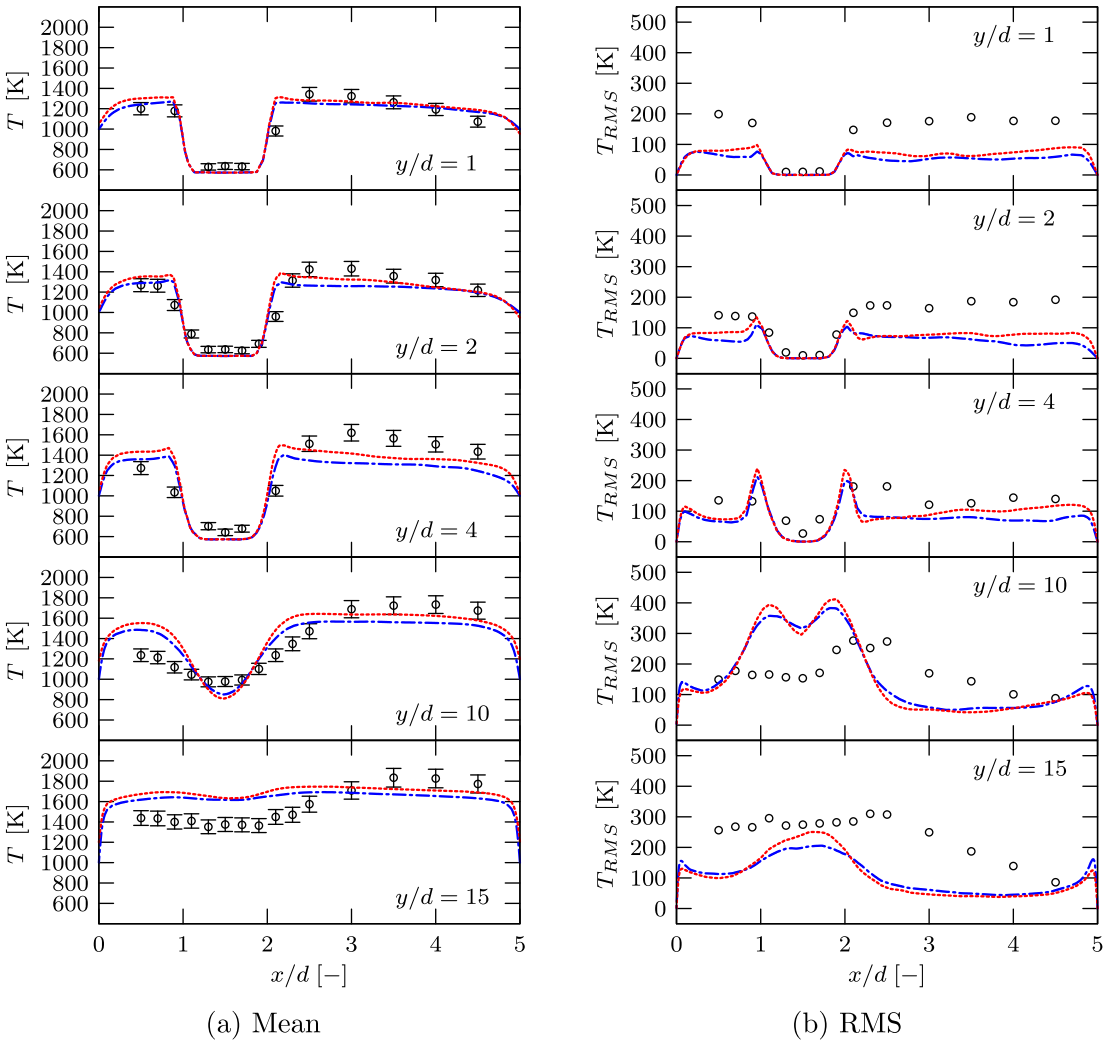

Fig. 8. Temperature profiles: Experiments (○), baseline case (-·-·-), non-uniform wall boundary condition (·····).

points at different locations in the domain. For instance, the data from a number of monitoring points in the fluid and solid close to the coupling interface at a streamwise location of $y/d = 10$ is presented. But similar effects can be observed at other streamwise locations. The exact locations of the different points is visualized in Fig. 10. The time series for this monitoring points are presented in Fig. 11a. The time series reveals high frequency and large amplitude oscillations for the monitoring points P_1 and P_2 which are located in the fluid at 2.5 mm and 1 mm distance to the fluid–solid interface. This oscillations are already significantly damped very close to the interface (P_3) and even further reduced inside the solid (P_4). At point P_5, all small scale oscillations are damped. Therefore, the penetration depth is very small and less than 0.5 mm. For points P_3, P_4 and P_5 a change of the mean temperature is observed. This could be either due to very large scale oscillations, which are not resolved in the relatively short time series, or due to different mean values compared to the DHT solution that has been used for initialization.

Similar information can be extracted from the corresponding Power Spectral Density (PSD) presented in Fig. 11b. The PSD of points P_1 and P_2 is almost identical and reveals significantly higher values compared to the other points for the entire frequency range. The PSD of point P_3 shows already significantly reduced values for all frequencies. The PSD of P_4 is only slightly lower than P_3. The graph for P_5 indicates almost no fluctuations any more. A frequency dependent damping behaviour can hardly be identified. The damping of the temperature fluctuations at the fluid–solid interface is similar for all resolved frequencies. However, the time series is too short to resolve frequencies below 5 Hz and potential low-pass characteristics are not captured.

In order to confirm the trends already described and further quantify the differences between the cases, the skin friction profiles in the streamwise direction are presented at the centre plane for the two short faces of the combustor walls in Fig. 12. The upper profile is located at the wall close to the jet and the lower profile at the wall with the large distance to the jet, where the recirculation zone is formed. The values are compared for the LES baseline case, the LES with non-uniform wall boundary condition and the fully coupled LES-CHT simulation. Following the Reynolds analogy for the shear stress and heat transfer, we can observe different heat exchange trends among the cases from the distribution of the skin friction. Especially for the wall where the large recirculation zone is located (see bottom plot of Fig. 12) the skin friction shows clear differences. This profile clearly indicates the location where the flow separates from the wall. All three approaches predict the same separation length, but they differ in terms of the strength, that is, the shear stress. The baseline case with uniform temperature underpredicts the shear stress compared to the other two cases, while the LES-CHT case shows a similar distribution to the case with non-uniform temperature distribution. This is consistent with

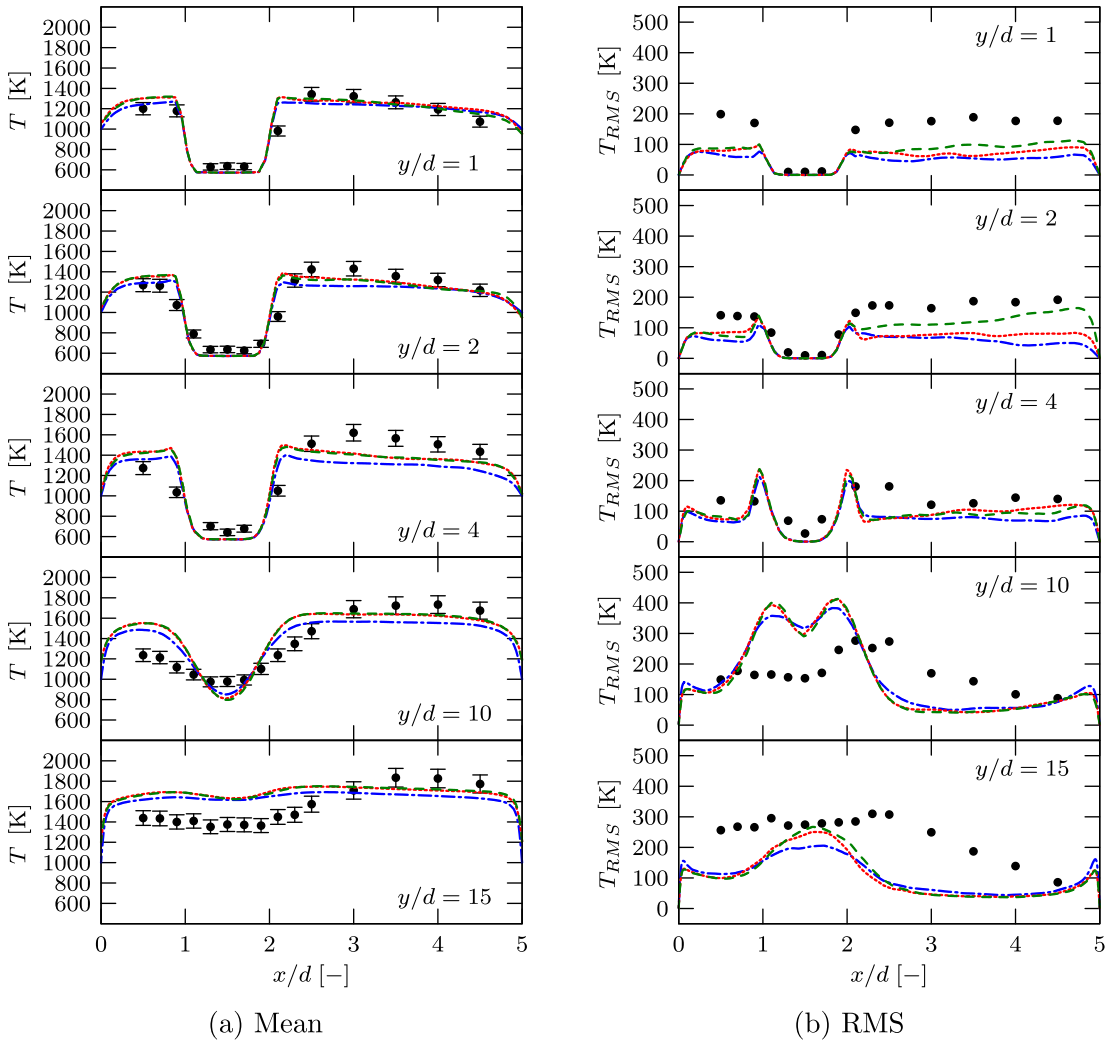

Fig. 9. Temperature profiles: Experiments (○), baseline case (------), non-uniform wall boundary condition (-·-·-), fully coupled CHT (– – –).

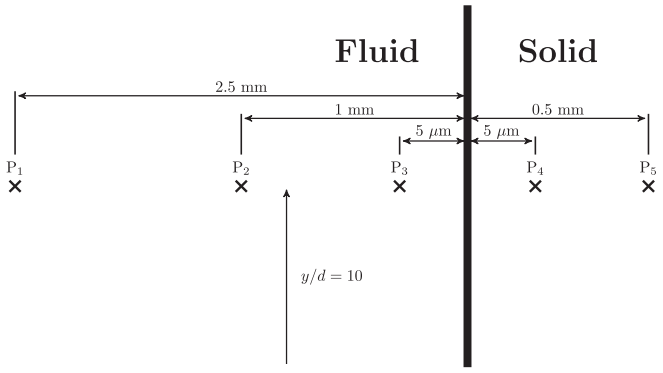

Fig. 10. Exact locations of the monitoring points.

the previous results where the effects of fluctuations near the wall for the CHT case have low influence on the mean velocity and temperature distributions.

5.4. Radiative heat transfer

Thermal radiation is one of the most important mechanisms of heat transfer in combustion devices [37]. However, in all previous investigations of the current test case, only convective heat transfer has been considered, while radiative heat transfer has been neglected. In this subsection, the impact of this simplification is examined by comparison of the baseline case, in which only convection is included, with a case in which radiation is additionally accounted for by the use of a radiation model based on the assumption of an optically thin flame as described in Section 2.1.

The resulting instantaneous radiation source term of the enthalpy equation is presented in Fig. 13. The dashed vertical lines indicate the streamwise locations at which the data for the detailed comparison with the experimental reference is extracted.

The radiative energy emitted by the gas shows the largest values in regions where both high temperatures and radiative species are present. Therefore, the highest source term values are observed in the post-flame region. The radiative energy emitted by the walls and absorbed by the gas is outbalanced by the radiation emitted by the gas phase in almost all regions of the combustion chamber. In the reactive layers of the flame, the radiation source term changes the sign. This is because in this region, some combustion products, and therefore the major radiative species, are already formed by chemical reaction but the local fluid temperature is still low and does not exceed the temperature of the surrounding walls. In this case, the absorption of radiative energy emitted by the walls exceeds the locally emitted radiative energy.

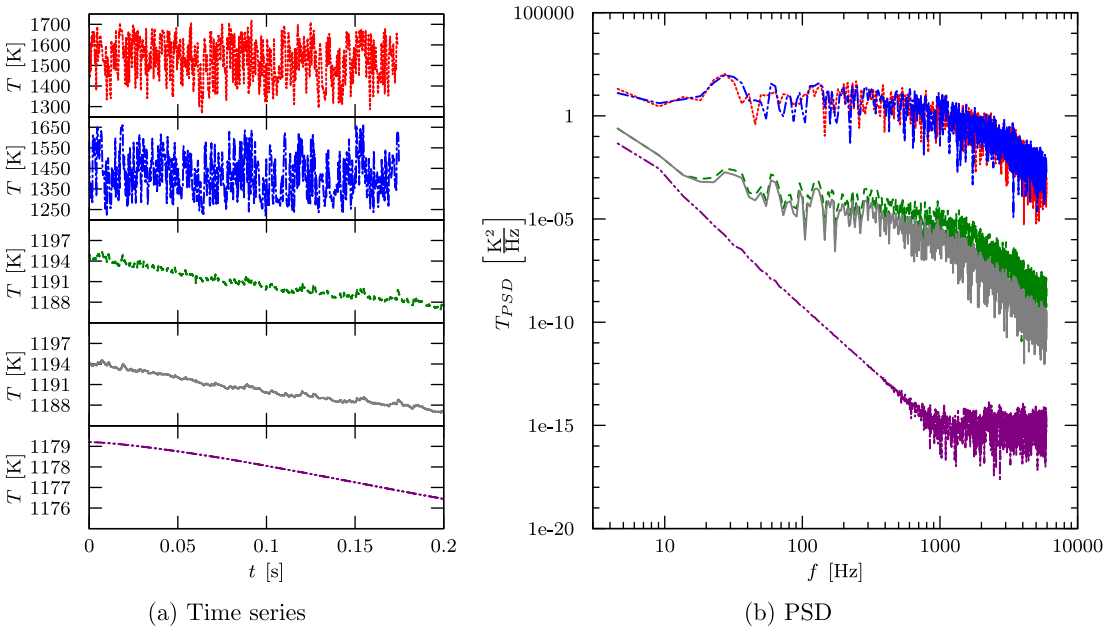

(a) Time series (b) PSD

Fig. 11. Time series and power spectral density for the near wall monitoring points at $y/d = 10$. P_1 (·····), P_2 (-·-·-), P_3 (– – –), P_4 (——), P_5 (-··-··-).

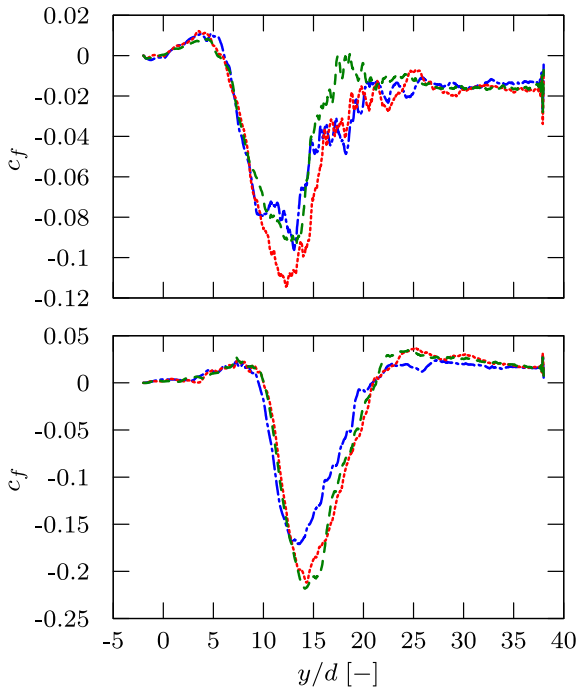

Fig. 12. Skin friction in streamwise direction at different locations around the combustor. Baseline case (-·-·-), non-uniform wall boundary condition (·····), fully coupled CHT (– – –).

The global influence of convective and radiative heat loss for the current case can be analysed by comparison of the integral heat loss values. The integral convective heat loss is determined by the heat flux to the quartz glass walls as:

$$\dot{Q}_c = \int_{A_w} \lambda \frac{\partial T}{\partial n}\bigg|_{wall} dA_w \tag{9}$$

where λ is the heat conductivity and A_w is the area of the wall. On the other hand, the radiative heat loss is determined by integrating the radiation source term over the combustion chamber volume V as:

$$\dot{Q}_R = \int_V \dot{q}_R dV \tag{10}$$

For the current case, the integral radiative heat loss is about 400 W and, therefore, almost by an order of magnitude lower than the integral heat loss by convection, which takes a value of about 3100 W. The heat losses to the walls of the combustor do not only account for convection but are also affected by the reduction of the temperature due to the radiative heat losses. This influence can be quantified by the comparison of the integral wall heat flux with the baseline case in which radiation is not considered. For that case, the integral convective flux is about 200 W higher compared to the radiation case. Therefore, the global influence of the radiative heat loss is further reduced.

The detailed influence of radiative heat transfer for this test case can be extracted from the temperature profiles presented in Fig. 14. The LES results including the radiation model are compared

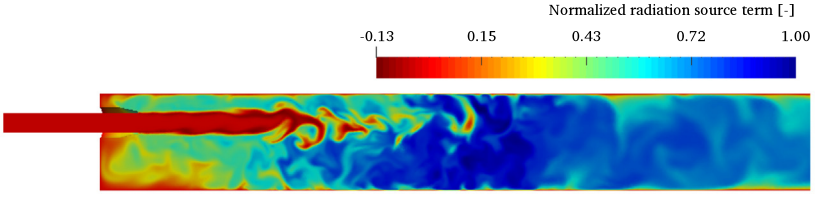

Fig. 13. Radiation source term normalized with maximum value (875149 W m^{-3}).

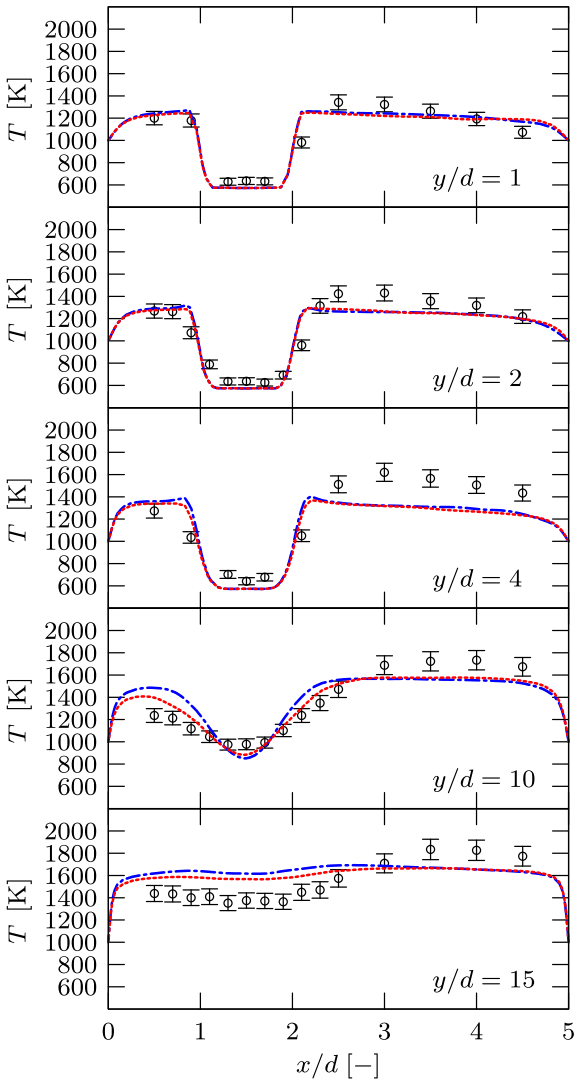

Fig. 14. Temperature profiles: Experiments (○), baseline case (-·-·-), radiation modelling based on optically thin gas assumption (·····).

to the experimental reference and the baseline case, in which radiation is neglected.

Only small differences between the temperature profiles of the simulations are observed in most regions of the combustion chamber. Especially in the recirculation regions, which are characterized by long residence times, convection is the major heat loss mechanism. Considering the reduction of the flow temperature from the adiabatic flame temperature of about 2050 K down to values of 1400–1600 K by convective heat transfer, the additional influence of radiation is negligibly small. However, the reactive layer is characterized by short residence times and a large distance to the walls. Under this conditions, the radiative heat transfer becomes an important heat transfer mechanism, under the condition that combustion products and high temperatures are already present. This is observed in the profile of $y/d = 10$ where the temperature in the shear layer of the flame is significantly reduced by radiation. As a consequence of the reduced temperature, the chemical reactions are slowed down and the spreading of the flame is increased. Furthermore, the slower chemical time scales lead to a slightly longer flame.

It can be concluded that the integral radiative heat loss is almost a magnitude smaller than the integral convective heat loss. In regions of high residence times the convective heat transfer is dominant and the impact of radiation on the temperature is negligibly small. However, in the reactive layer a distinctive influence of radiative heat transfer is observed that affects the spreading and the length of the flame.

6. Conclusions

In this work, the effect of different heat transfer mechanisms and thermal conditions for the chamber walls of a turbulent jet flame configuration is investigated in detail by means of numerical simulations. The influence of radiation, convection and heat conduction over the solid walls is examined by comparing the gas temperature with reference experimental data.

The study presents a novel methodology based on a Dual Heat Transfer (DHT) approach in combination with RANS turbulence treatment to compute steady fields at the fluid–solid interface. Boundary values of 800, 900 and 1000 K are applied to the outer solid wall in the DHT approach to investigate the influence of the external walls on the gas temperature inside the combustion chamber. It is shown that the variation of the outer wall temperature affects the overall gas temperature inside the combustion chamber and the prediction of the flame length, but the influence on flame dynamics and temperature distribution within the combustion chamber is minor at most locations. It can therefore be concluded that the variation of the temperature due to the different wall boundary conditions is too small to significantly affect the chemical kinetics. However, a significant variation of the temperature along the combustor walls of about 450 K is found with peak values at the flame location and cold regions further downstream and upstream of the recirculation zone where the convective heat losses are significant due to long residence times of the fluid. In conclusion, the assumption of a uniform temperature boundary condition is not accurate for this configuration.

In a second step, the influence of a non-uniform temperature distribution is assessed by comparing LES results with the baseline case with fixed temperature at walls. Thereby, the temperature underprediction in the hot regions is reduced by about 100 K. However, the flame length and shape remains almost unaffected. The predicted RMS values of the temperature are slightly increased in the recirculation zone, leading to an improved agreement with the experiments. It is remarkable that the large spatial variation of the wall temperature only has a limited impact on the temperature prediction inside the combustion chamber.

In order to assess the transient characteristics of the coupled fluid–solid problem, a strongly coupled LES-Conjugate Heat Transfer (CHT) simulation is carried out. In this approach, similar mean fields are predicted in the combustion chamber compared to the stand-alone LES simulation with non-uniform wall temperature. However, the prediction of the RMS values is significantly improved in the recirculation region for the upstream profiles. A maximum difference of about 80 K is observed by application of the relaxed thermal boundary condition. The analysis of monitoring points at different positions from the walls indicates that the turbulent temperature fluctuations are damped by the solid. The thermal activity ratio of the fluid–solid interface is small, which means that the characteristic boundary behaviour tends towards an isothermal condition. For the resolved frequency range, no frequency dependent damping is observed but all frequencies are damped similarly.

In a last step, the influence of radiation as an additional heat loss mechanism is analysed by inclusion of a radiation model. Even though a comparison of the integral heat loss values reveals that the convective losses exceed the radiative value by an order of magnitude in this case, distinctive differences are found in the comparison to the baseline case. While the temperature profiles

are hardly affected by radiation in regions with long residence time, the flame spreading is significantly increased by inclusion of the radiation model and improves the comparison to the experimental reference data. This can be explained by the fact that radiation is low in magnitude in burnt gas zones with large residence times, but significant in the high temperature area at the flame front. It can be concluded that radiation modelling only significantly affects the temperature prediction for configurations in which the high temperature gases are not substantially cooled by convective heat loss.

Acknowledgements

The research leading to these results has received funding through the People Programme (Marie Curie Actions) of the European Union's Seventh Framework Programme (FP7, 2007–2013) under the Grant agreement No. FP7-290042 for the project COPA-GT as well as the European Union's Horizon 2020 Programme (2014–2020) and from Brazilian Ministry of Science, Technology and Innovation through Rede Nacional de Pesquisa (RNP) under the HPC4E Project, Grant agreement No. 689772. The authors thankfully acknowledge the computer resources, technical expertise and assistance provided by the Red Española de Supercomputación (RES). Finally, the authors would like to thank O. Lammel for the useful discussions and kindly providing the data for the comparison.

References

[1] A. Misdariis, O. Vermorel, T. Poinsot, LES of knocking in engines using dual heat transfer and two-step reduced schemes, Combust. Flame (2015).
[2] A.D. Sa, S.A. Zubaidy, Gas turbine performance at varying ambient temperature, Appl. Therm. Eng. 31 (2011) 2735–2739.
[3] H. Canire, A. Willockx, E. Dick, M.D. Paepe, Raising cycle efficiency by intercooling in air-cooled gas turbines, Appl. Therm. Eng. 26 (2006) 1780–1787.
[4] Y. Li, S.-C. Kong, Coupling conjugate heat transfer with in-cylinder combustion modeling for engine simulation, Int. J. Heat Mass Transfer 54 (2011) 2467–2478.
[5] O. Lammel, M. Stöhr, P. Kutne, C. Dem, W. Meier, M. Aigner, Experimental analysis of confined jet flames by laser measurement techniques, J. Eng. Gas Turbines Power 134 (2012).
[6] S. Gövert, D. Mira, J. Kok, M. Vzquez, G. Houzeaux, Turbulent combustion modelling of a confined premixed jet flame including heat loss effects using tabulated chemistry, Appl. Energy 156 (2015) 804–815.
[7] F. Proch, A. Kempf, Modeling heat loss effects in the large eddy simulation of a model gas turbine combustor with premixed flamelet generated manifolds, Proc. Combust. Inst. 35 (2015) 3337–3345.
[8] A. Donini, S. Martin, R. Bastiaans, J. van Oijen, L. de Goey, Numerical simulations of a premixed turbulent confined jet flame using the flamelet generated manifold approach with heat loss inclusion, in: Proc. ASME Turbo Expo, San Antonio, Texas, 2013.
[9] A. Fancello, L. Panek, O. Lammel, W. Krebs, R. Bastiaans, L. de Goey, Turbulent combustion modeling using flamelet-generated manifolds for gas turbine applications in openfoam, in: Proceedings of the ASME Turbo Expo 2014, Düsseldorf, Germany, 2014.
[10] K. Claramunt, R. Cnsul, C. Prez-Segarra, A. Oliva, Multidimensional mathematical modeling and numerical investigation of co-flow partially premixed methane/air laminar flames, Combust. Flame 137 (2004) 444–457.
[11] J. van Oijen, F. Lammers, L. de Goey, Modeling of complex premixed burner systems by using flamelet-generated manifolds, Combust. Flame 127 (2001) 2124–2134.
[12] O. Gicquel, N. Darabiha, D. Thevenin, Laminar premixed hydrogen/air counterflow flame simulations using flame prolongation of ILDM with differential diffusion, Proc. Combust. Inst. 28 (2000) 1901–1908.
[13] R. Kee, F. Rupley, J. Miller, M. Coltrin, J. Grcar, E. Meeks, H. Moffat, A. Lutz, G. Dixon-Lewisa, M. Smooke, J. Warnatz, G. Evans, R. Larson, R. Mitchell, L. Petzold, W. Reynolds, M. Caracotsios, W. Stewart, P. Glarborg, C. Wang, O. Adigun, Chemkin collection, release 3.6, 2000.
[14] R. Kee, G. Dixon-Lewis, J. Warnatz, M. Coltrin, J. Miller, A fortran computer code package for the evaluation of gas-phase multicomponent transport properties, Technical Report SAND86-8246, Sandia National Laboratories, 1986.
[15] G. Smith, D. Golden, M. Frenklach, N. Moriarty, B. Eiteneer, M. Goldenberg, C.T. Bowman, R. Hanson, S. Song, W. Gardiner, V. Lissianski, Z. Qin, GRI-Mech 3.0, 1999, URL: <http://www.me.berkeley.edu/gri-mech/>.
[16] D. Cecere, E. Giacomazzi, F. Picchia, N. Arcidiacono, F. Donato, R. Verzicco, A non-adiabatic flamelet progress variable approach for les of turbulent premixed flames, Flow Turbul. Combust. 86 (2011) 667–688.
[17] B. Fiorina, R. Baron, O. Gicquel, D. Thevenin, S. Carpentier, N. Darabiha, Modelling non-adiabatic partially premixed flames using flame-prolongation of ildm, Combust. Theor. Model. 7 (2003) 449–470.
[18] P. Domingo, L. Vervisch, S. Payet, R. Hauguel, Dns of a premixed turbulent v flame and les of a ducted flame using a fsd-pdf subgrid scale closure with fpi-tabulated chemistry, Combust. Flame 143 (2005) 566–586.
[19] J. Kok, J. Louis, J. Yu, The irst model for turbulent premixed non-adiabatic methane flames, Combust. Sci. Technol. 149 (1999) 225–247.
[20] D. Mira, X. Jiang, C. Moulinec, D. Emerson, Numerical assessment of subgrid scale models for scalar transport in large-eddy simulations of hydrogen-enriched fuels, Int. J. Hydrogen Energy 39 (2014) 7173–7189.
[21] F. Nicoud, F. Ducros, Subgrid-scale stress modelling based on the square of the velocity gradient, Flow Turb. Combust. 62 (1999) 183–200.
[22] F. Menter, Two-equation eddy-viscosity turbulence models for engineering applications, AIAA J. 32 (1994) 1598–1605.
[23] C. Tien, Thermal radiation properties of gases, in: T. Irvine, J. Hartnett (Eds.), Advances in Heat Transfer, vol. 5, Academic Press, New York, 1968, pp. 253–324.
[24] R. Barlow, A. Karpetis, J. Frank, J.-Y. Chen, Scalar profiles and {NO} formation in laminar opposed-flow partially premixed methane/air flames, Combust. Flame 127 (2001) 2102–2118.
[25] J.Y. Chen, Y. Liu, B. Rogg, Reduced Kinetic Mechanisms for Applications in Combustion Systems, Springer Berlin Heidelberg, Berlin, Heidelberg, 1993, pp. 196–223.
[26] K. Kelley, High-temperature heat-content, heat-capacity, and entropy data for the elements and inorganic compounds, Bulletin (United States. Bureau of Mines) 584, U.S. Govt. Print. Off., 1960.
[27] O. Sergeev, A. Shashkov, A. Umanskii, Thermophysical properties of quartz glass, J. Eng. Phys. 43 (1982) 1375–1383.
[28] EN 1993-1-2, Annex C, Eurocode 3: Design of steel structures - Part 1-2: General rules - Structural fire design, Standard, European Committee for Standardization, 2005.
[29] D. Mira, M. Zavala-Ake, M. Avila, H. Owen, J.C. Cajas, M. Vazquez, G. Houzeaux, Heat transfer effects on a fully premixed methane impinging flame, Flow Turbul. Combust. (2016) 1–23.
[30] G. Gimenez, M. Errera, D. Baillis, Y. Smith, F. Pardo, A coupling numerical methodology for weakly transient conjugate heat transfer problems, Int. J. Heat Mass Transfer 97 (2016) 975–989.
[31] O. Lammel, personal communication, Oct. 2015.
[32] BSC-CNS, Alya multiphysics code, 2014, URL: <http://www.bsc.es/computer-applications/alya-system>.
[33] G. Houzeaux, J. Principe, A variational subgrid scale model for transient incompressible flows, Int. J. Comput. Fluid D. 22 (2008) 135–152.
[34] M. Vazquez, G. Houzeaux, S. Koric, A. Artigues, J. Aguado-Sierra, R. Aris, D. Mira, H. Calmet, F. Cucchietti, H. Owen, A. Taha, J.M. Cela, Alya: Towards exascale for engineering simulation codes, in: International Supercomputing Conference 2014, arXiv:1404.4881[physics.comp-ph], 2014.
[35] M. Shahi, J.B. Kok, J.R. Casado, A.K. Pozarlik, Transient heat transfer between a turbulent lean partially premixed flame in limit cycle oscillation and the walls of a can type combustor, Appl. Therm. Eng. 81 (2015) 128–139.
[36] A. Chatelain, F. Ducros, O. Métais, Direct and Large-Eddy Simulation V, in: Proceedings of the fifth international ERCOFTAC Workshop on direct and large-eddy simulation held at the Munich University of Technology, August 27–29, 2003, Springer, Netherlands, Dordrecht, 2004, pp. 307–314, http://dx.doi.org/10.1007/978-1-4020-2313-2_33, URL: http://dx.doi.org/10.1007/978-1-4020-2313-2_33.
[37] D.H.M. F Modest, Radiative Heat Transfer in Turbulent Combustion Systems: Theory and Applications, Springer International Publishing, 2016.